Computers, Materials & Continua

Tech Science Press

Doi:10.32604/cmc.2025.068360

ARTICLE

Sine-Polynomial Chaotic Map (SPCM): A Decent Cryptographic Solution for Image Encryption in Wireless Sensor Networks

David S. Bhatti[1,*], **Annas W. Malik**[2], **Haeung Choi**[1] **and Ki-Il Kim**[3,*]

[1]School of Electrical Engineering and Computer Science, Gwangju Institute of Science and Technology (GIST), Gwangju, 61005, Republic of Korea

[2]Faculty of Information Technology & Computer Science, University of Central Punjab, Lahore, 54000, Pakistan

[3]Department of Computer Science and Engineering, Chungnam National University, Daejeon, 34134, Republic of Korea

*Corresponding Authors: David S. Bhatti. Email: david.bhatti@gist.ac.kr; Ki-Il Kim. Email: kikim@cnu.ac.kr

Received: 27 May 2025; Accepted: 25 July 2025; Published: 29 August 2025

ABSTRACT: Traditional chaotic maps struggle with narrow chaotic ranges and inefficiencies, limiting their use for lightweight, secure image encryption in resource-constrained Wireless Sensor Networks (WSNs). We propose the SPCM, a novel one-dimensional discontinuous chaotic system integrating polynomial and sine functions, leveraging a piecewise function to achieve a broad chaotic range ($r \in [0, 12]$) and a high Lyapunov exponent (5.04). Validated through nine benchmarks, including standard randomness tests, Diehard tests, and Shannon entropy (3.883), SPCM demonstrates superior randomness and high sensitivity to initial conditions. Applied to image encryption, SPCM achieves 0.152582 s (39% faster than some techniques) and 433.42 KB/s throughput (134% higher than some techniques), setting new benchmarks for chaotic map-based methods in WSNs. Chaos-based permutation and exclusive or (XOR) diffusion yield near-zero correlation in encrypted images, ensuring strong resistance to Statistical Attacks (SA) and accurate recovery. SPCM also exhibits a strong avalanche effect (>50% bit difference), making it an efficient, secure solution for WSNs in domains like healthcare and smart cities.

KEYWORDS: Chaos theory; chaotic system; image encryption; cryptography; wireless sensor networks (WSNs)

1 Introduction

WSNs have emerged as a fundamental component of numerous applications, including environmental monitoring, healthcare, industrial automation, and smart city infrastructure, where real-time transmission of sensitive data, such as images, is critical. These networks consist of spatially distributed, resource-constrained sensor nodes that operate with limited computational power, battery energy, and bandwidth [1]. Traditional encryption schemes, such as AES, RSA, PKI though robust, are computationally intensive and often impractical in WSN environments due to their high energy and processing demands [2]. This necessitates the development of lightweight and efficient cryptographic techniques specifically tailored for WSNs.

1.1 Wireless Sensor Networks (WSNs)

WSNs are specialized wireless ad hoc networks composed of low-power sensor nodes capable of sensing, processing, and wirelessly communicating data. These networks enable real-time monitoring of various physical phenomena such as temperature, humidity, pressure, motion, and even physiological signals. WSNs are widely adopted across domains including defense, agriculture, healthcare, industrial automation, and

Copyright © 2025 The Authors. Published by Tech Science Press.
This work is licensed under a Creative Commons Attribution 4.0 International License, which permits unrestricted use, distribution, and reproduction in any medium, provided the original work is properly cited.

smart urban infrastructure [1]. Their self-configuring, scalable, and fault-tolerant nature makes them ideal for deployment in dynamic or harsh environments. Fig. 1 summarizes major application areas of WSNs.

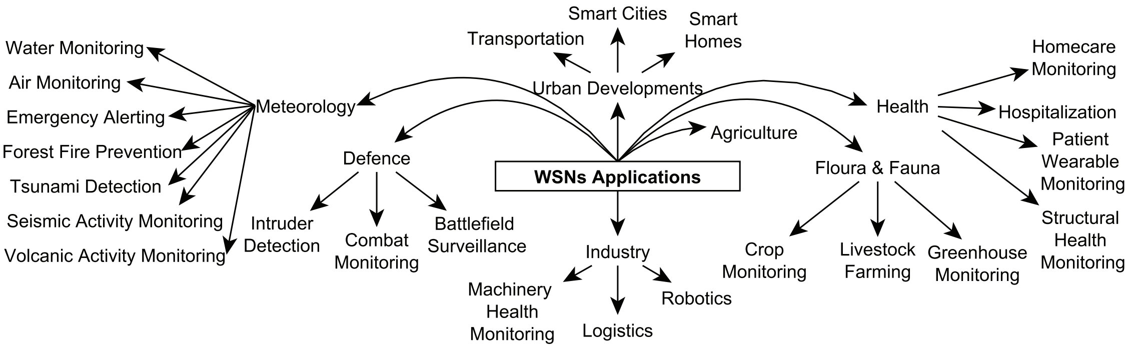

Figure 1: Major application domains of WSNs

Despite their wide applicability, WSNs face two critical challenges: resource constraints and security vulnerabilities. Sensor nodes are typically powered by non-replaceable batteries and expected to function over extended periods. Their limited processing power and memory severely restrict the use of complex cryptographic algorithms. Additionally, their communication relies on open wireless channels, making them susceptible to attacks such as eavesdropping, spoofing, and denial-of-service [3]. Therefore, energy-aware and lightweight cryptographic mechanisms are essential for securing data without compromising network longevity. A typical WSN architecture, as shown in Fig. 2, consists of a large number of sensor nodes randomly deployed in the target area. These nodes communicate with a base station (sink), which acts as a central data aggregator. Queries from the sink are propagated through the network, and responses from matching sensor nodes are transmitted back. To optimize energy usage, a cluster-based model is often employed where selected nodes act as cluster heads. These heads are responsible for aggregating, compressing, and securely transmitting data to the sink. Users retrieve the data from the sink through backhaul communication (e.g., satellite or cellular links) [4].

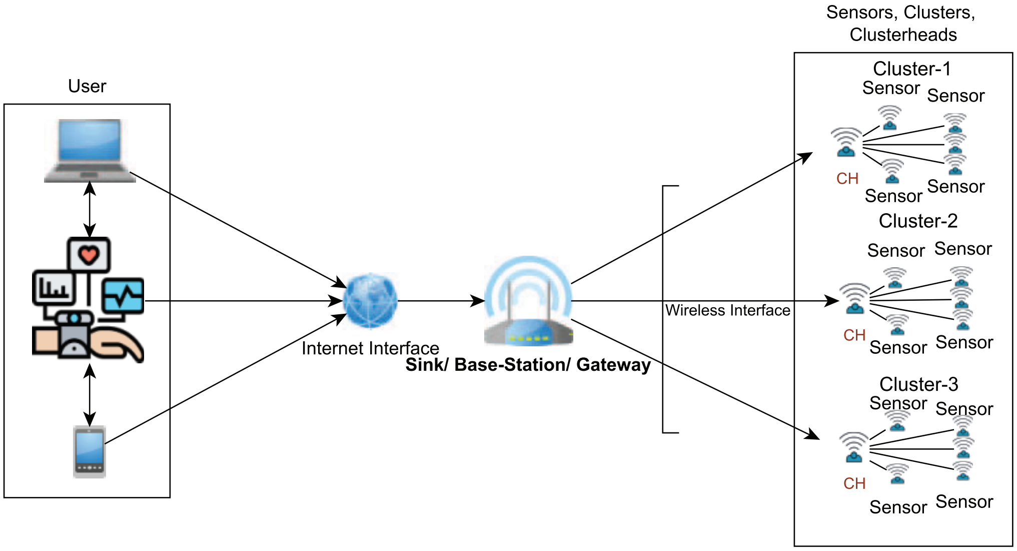

Figure 2: Typical architecture of WSN

1.2 Chaotic Maps

Chaotic systems, pioneered by Poincaré, Lorenz, and others, exhibit unpredictable behavior despite being deterministic, due to their sensitivity to initial conditions [5,6]. Their properties, such as topological mixing, dense periodic orbits, and fractal geometry, make them well-suited for cryptography, offering complex dynamics and strong key sensitivity [7,8]. One-dimensional chaotic maps are especially useful for generating complex pseudo-random sequences in lightweight encryption schemes for WSNs [9,10]. These systems are modeled as: $z_{(m+1)} = f(z_m)$, where $f(z_m)$ maps the current state z_m to the next state $z_{(m+1)}$, starting from an initial condition z_0. This simple yet powerful formulation captures the dynamic and intricate behavior of one-dimensional chaotic systems, balancing simplicity and complexity for applications across various fields [11]. Chaotic maps are discrete dynamical systems widely studied for their complex, unpredictable behavior despite simple mathematical formulations. This study focuses on one-dimensional maps $f : [0,1] \to [0,1]$, which balance analytical tractability with rich dynamics. Three classical chaotic maps (Logistic, Tent, and Sine) are foundational to understanding chaos and serve as the basis for advanced applications like encryption and secure communication. The Logistic Map is defined as: $z_{(m+1)} = a \cdot z_m \cdot (1 - z_m)$, where $z_m \in [0,1]$ and $a \in [0,4]$. It exhibits chaos for $a \in [3.57,4]$, characterized by sensitivity to initial conditions, as confirmed by a positive Lyapunov Exponent (LE) and visualized in its bifurcation diagram [12]. The Tent Map is a piecewise function given by:

$$z_{(m+1)} = \begin{cases} u \cdot z_m & \text{for } z_m < 0.5, \\ u \cdot (1 - z_m) & \text{for } z_m \geq 0.5, \end{cases} \tag{1}$$

with $u \in (1,2]$. Chaotic behavior strengthens as $u \to 2$, with sequences covering $[0,1]$, and is supported by its LE [12]. The Sine Map is expressed as: $z_{(m+1)} = r \cdot \sin(\pi \cdot z_m)$, where $r \in [0,1]$. It produces chaos for $r \in [0.867,1]$, with increasing chaoticity as $r \to 1$ [12].

To address energy and security constraints in WSNs, this study proposes a lightweight image encryption framework based on the SPCM a one-dimensional system that combines sinusoidal and polynomial terms to overcome the limitations of classical maps, including restricted key space and weak randomness [13]. The SPCM offers high chaotic complexity with low computational cost, making it ideal for WSNs. In the proposed model, modulo 1 operation is performed using basic thumb of rule that is $x \bmod y = x - y \cdot \left\lfloor \frac{x}{y} \right\rfloor$ (e.g., $1.5 \mod 1 \triangleq 0.5$); it also holds for integer modulo (e.g., $258 \mod 256 \triangleq 2$). Integrated with permutation and XOR-based diffusion, the scheme ensures strong security and energy efficiency, outperforming existing methods across multiple chaos and encryption benchmarks.

1.3 Motivation and Contributions

The key contributions of this research are given below:

1. We propose SPCM, a discontinuous one-dimensional map combining polynomial and sine dynamics. It expands the chaotic range, boosts key sensitivity, and enhances robustness, making it suitable for secure image encryption in resource-limited WSNs.
2. SPCM is rigorously evaluated using nine benchmarks, including bifurcation, Lyapunov exponents (5.04), Shannon entropy (3.883), sensitivity, cobweb plots, 0-1 test, histograms, and NIST/Diehard randomness tests. It shows superior chaos, broader stability, and stronger randomness, outperforming prior methods assessed with 2–7 metrics.
3. Designed for image encryption in WSNs, SPCM offers lightweight, secure encryption with low computational load. Its chaos-based keying, permutation, and XOR diffusion resist SA, reduce energy use, and support reliable data recovery.

The rest of the manuscript is organized as follows: Section 2 Related Work; Section 3 Proposed Sine-Polynomial Chaotic System; Section 4 Analysis and Discussion; Section 5 Application; Section 6 Limitations; Section 7 Conclusion.

2 Related Work

This section explores recent advancements in chaotic systems, reviewing methodologies, strategies, and theoretical foundations aimed at refining their properties for diverse applications.

Lambić [14] proposed a one-dimensional Chaotic Map using integer multiplication and circular shifts, optimized for memory-limited devices but potentially restrictive for encryption. Shafique [15] employed the Cubic-Logistic map for S-box construction to enhance cryptographic properties, though its smaller key space and computational complexity may limit practical usability.

Zhang et al. [16] introduced an image encryption algorithm leveraging a hyperchaotic system and the variable-step Josephus problem, using pseudorandom sequences for scrambling and pixel-wise encryption. It achieves high entropy (7.997) and low correlation (±0.01), ensuring robust security. Ali et al. [17] proposed a color image encryption scheme with chaotic maps, involving permutation, chaotic S-box substitution, and XOR-based diffusion. While secure, its computational complexity may hinder use in resource-limited settings like WSNs.

Li et al. [18] proposed the Logistic-Tent-Sine Chaotic Map (LTSS) for cloud image security, offering improved chaotic behavior, though remaining vulnerable to certain attacks. Fadhil et al. [19] used the 1D logistic map for S-box design, though its narrow key space may weaken security. Cheng et al. [20] introduced the 1D-TPSC Chaotic System for image encryption, demonstrating strong dynamics but facing scalability and adaptability challenges.

Zhang et al. [21] developed an image encryption algorithm using 1D and 2D logistic chaotic systems, leveraging initial value sensitivity and pseudo-randomness. However, fixed-length keys and sequential processes may limit its suitability for large datasets or real-time applications, with a narrow key space reducing resistance to sophisticated cryptanalytic attacks. Mondal and Singh [22] proposed a lightweight chaotic encryption scheme for IoT devices, using bit-wise permutation and substitution in a single scan for efficiency. Its simplicity, while suitable for low-power settings, may compromise resilience against sophisticated cryptanalytic attacks.

Liu and Wang [23] proposed a cluster of 1D quadratic Chaotic Maps for image encryption, expanding the parameter space to enhance security. However, relying solely on the 1D quadratic map may introduce vulnerabilities. Chen et al. [24] introduced a digital image encryption algorithm using a splicing model and quaternary coding, improving attack resistance. Despite a large key space, potential weaknesses in chaotic dynamics and cryptanalysis susceptibility may impact long-term security.

Alexan et al. [25] presented a color image encryption algorithm combining the KAA map with multiple chaotic maps, utilizing Shannon's principles of security through bit confusion and diffusion. Confusion is achieved using two encryption keys generated from different chaotic maps, while diffusion is implemented using the KAA map. The algorithm is shown to be robust, efficient, and resistant to various attacks, passing all tests in the NIST SP 800 suite.

Ding et al. [26] introduced memristive Chaotic Systems using 1D Chaotic Maps for randomness, but high computational overhead limits practicality. Malik et al. [27] proposed an S-box using the Tent-Sine (TS) Chaotic System, enhancing the chaotic range for cryptography. Despite reduced chaoticity at certain bifurcation points, extensive analysis confirms its cryptographic strength.

Alawida [28] proposed an Enhanced Logistic Map (ELM) for secure random number generation, improving randomness via chaotic perturbations, though its deterministic nature may pose cryptanalytic risks. Jain et al. [29] introduced MMCBIE, a multi-chaotic map image encryption scheme for IoT, combining Henon and 2D-Logistic maps to achieve high confusion and diffusion, validated by metrics like NPCR and UACI. However, its complexity may challenge IoT devices. Kiran [30] proposed a GPU-accelerated chaos-based encryption scheme using CUDA parallelization, demonstrating enhanced throughput for mobile applications. While effective for GPU-enabled devices, its computational demands exceed typical WSN node capabilities. Archana et al. [31] developed a blockchain-based medical image encryption scheme for IoT-Edge systems, using chaotic maps and optimized key generation on Ethereum, demonstrating strong security via NIST tests, though its computational overhead may limit real-time edge applications. A novel triple image encryption scheme using chaotic measurement matrices, Josephus scrambling, and 3D wavelet transform-based embedding was proposed by Hu et al. [32] to achieve high visual security and reconstruction quality without carrier data for decryption, surpassing existing methods.

While WSNs demand lightweight security solutions, traditional cryptographic approaches face three critical limitations in resource-constrained environments [33]: 1) the computational overhead of AES/RSA operations exceeds typical WSN node capabilities [34,35], 2) key management in PKI-based systems creates unsustainable energy costs [26], and 3) block cipher modes introduce latency incompatible with real-time applications [17]. Chaotic maps have emerged as a promising alternative [25], offering deterministic pseudo-randomness for lightweight key generation [16], single-pass processing efficiency, and inherent resistance to side-channel attacks [18]. However, existing 1D chaotic systems remain limited by narrow parameter ranges (e.g., $r \in [3.57, 4]$ for Logistic maps [27]) and suboptimal Lyapunov exponents.

Chaotic systems like hyperchaotic and lightweight schemes offer high entropy and strong security for image encryption. However, in WSNs, they face compounded challenges: multi-map schemes and complex S-boxes increase computational load while restricting key space, and oversimplified lightweight designs often sacrifice robustness. These unresolved limitations motivate our search for a chaotic system that simultaneously achieves WSN compatibility (minimal computational/energy overhead) and strong security (high Lyapunov exponents, wide chaotic ranges). Moreover, wireless visual sensor networks (WVSNs) have emerged as a recent research focus. While Liu et al. [36] proposed a framework for improving coverage estimation in irregular, obstacle-rich environments, our proposed SPCM system complements it by securing captured visual data through efficient, lightweight chaotic encryption. Together, they address both reliable sensing and robust data protection in resource-constrained WVSNs.

3 Proposed SPCM

One-dimensional discontinuous maps are vital in modeling dynamical systems with abrupt behavioral transitions across phase space regions. Defined by piecewise functions, these systems switch dynamics based on the state variable's position, expressed as:

$$f(m,n,\rho) = \begin{cases} f_1(m,n,\rho), & \text{for } (m,n) \in Q_1 \\ f_2(m,n,\rho), & \text{for } (m,n) \in Q_2 \\ \vdots & \\ f_n(m,n,\rho), & \text{for } (m,n) \in Q_n \end{cases} \tag{2}$$

Here $Q_1, Q_2, \ldots, Q_n$ denote distinct phase space regions, and ρ is a control parameter. These maps effectively capture complex bifurcations and chaotic dynamics. The sine-polynomial chaotic system is a novel one-dimensional discontinuous map operating in $(0,1)$, defined as a piecewise function with control a parameter $r \in [0, 12]$. For $x_n \in (0, 0.5)$, the system evolves as $(4 \cdot \sin(2\pi x_n r) + x_n^3) \mod 1$; for $x_n \in [0.5, 1)$, it follows $(4 \cdot \sin(2\pi x_n r) + (1 - x_n^2)) \mod 1$. This design ensures distinct chaotic dynamics across the interval.

$$x_{(n+1)} = \begin{cases} (4 \cdot \sin(2\pi x_n r) + x_n^3) \mod 1, & \text{if } 0.0 < x_n < 0.5 \\ (4 \cdot \sin(2\pi x_n r) + (1 - x_n^2)) \mod 1, & \text{if } 0.5 \le x_n < 1.0 \end{cases} \tag{3}$$

The piecewise sine-polynomial formulation in Eq. (3) combines cubic polynomial terms (x_n^3 for $x_n < 0.5$ and $1 - x_n^2$ for $x_n \geq 0.5$) with a sinusoidal component ($4\sin(2\pi x_n r)$) to achieve three cryptographic advantages: 1) the polynomials introduce asymmetric nonlinearity while preventing predictable behavior, 2) the sine function ensures ergodicity and sensitivity to both initial conditions (x_0) and control parameter (r), and 3) the deliberate discontinuity at $x_n = 0.5$ enhances trajectory mixing. This synthesis outperforms classical maps by extending the chaotic range to $r \in [0, 12]$ while maintaining computational efficiency critical for WSNs [37].

The sine-polynomial chaotic system generates complex, unpredictable trajectories with high sensitivity to initial conditions. Unlike traditional logistic and tent maps, which have limited chaotic ranges and periodic windows, the SP system combines the oscillatory sine function and nonlinear polynomial terms to enhance sequence complexity. A discontinuity at $x_n = 0.5$ ensures diverse dynamics. The modulo 1 operation is defined as: $x \bmod y = x - y \cdot \left\lfloor \frac{x}{y} \right\rfloor$. Here, $x \in \left\{4 \cdot \sin(2\pi x_n r) + x_n^3, \quad 4 \cdot \sin(2\pi x_n r) + (1 - x_n^2)\right\}$ (see Eq. (3)), $y = 1$ is the divisor, and $\lfloor \cdot \rfloor$ denotes the floor function. The modulo 1 operation confines outputs to the interval $(0, 1)$, wrapping values, such as 1.9 mod 1 = 0.9, to ensure consistent chaotic behavior.

Furthermore, an increased control parameter range ($r \in [0, 12]$) extends the system's flexibility, enabling a broader spectrum of chaotic behaviors. This is valuable for applications requiring fine-tuned chaos, such as cryptographic key generation and secure communications. The dual-equation structure maintains high sensitivity to initial conditions across the domain, a hallmark of robust chaotic maps.

The development of proposed chaotic systems is motivated by the need for greater dynamical richness and wider parameter ranges. The proposed sine-polynomial system addresses this by offering a control parameter r up to 12, allowing exploration of more intricate dynamics and applications, which require enhanced variability and sensitivity.

4 Analysis and Discussion on Proposed SPCM

The proposed SPCM is evaluated in three domains: *Chaotic Behavior Evaluation* (bifurcation, Lyapunov exponents, sensitivity, cobweb diagrams, 0–1 tests, histograms, ergodicity, mixing), *NIST SP800-22R1A*, and *Diehard tests*. Results confirm high sensitivity, strong chaotic behavior, and compliance with cryptographic randomness standards. Parameters $x_0 = 0.2827727272727267$ and $r = 11.8843888888888877$ were chosen for maximal chaos.

4.1 Chaotic Behavior Evaluation

The Lyapunov exponent (λ) [38] quantifies chaos via the divergence of trajectories: $\Delta(t) \sim \Delta(0)e^{\lambda t}$. Positive λ indicates chaos. For 1D maps:

$$\lambda = \lim_{n \to \infty} \frac{1}{n} \sum_{i=1}^{n} \log |f'[x_i]| . \tag{4}$$

The derivative $f'(x_n)$ for the proposed map (Eq. (3)) is:

$$f'(x_n) = \begin{cases} 8\pi r \cdot \cos(2\pi x_n/r) + 3x_n^2, & 0 < x_n < 0.5, \\ 8\pi r \cdot \cos(2\pi x_n/r) - 2x_n, & 0.5 \le x_n < 1. \end{cases} \tag{5}$$

λ is computed by averaging $\log|f'(x_n)|$ over iterations. For clarity, the Lyapunov exponent computation process is illustrated in the flowchart shown in Fig. 3.

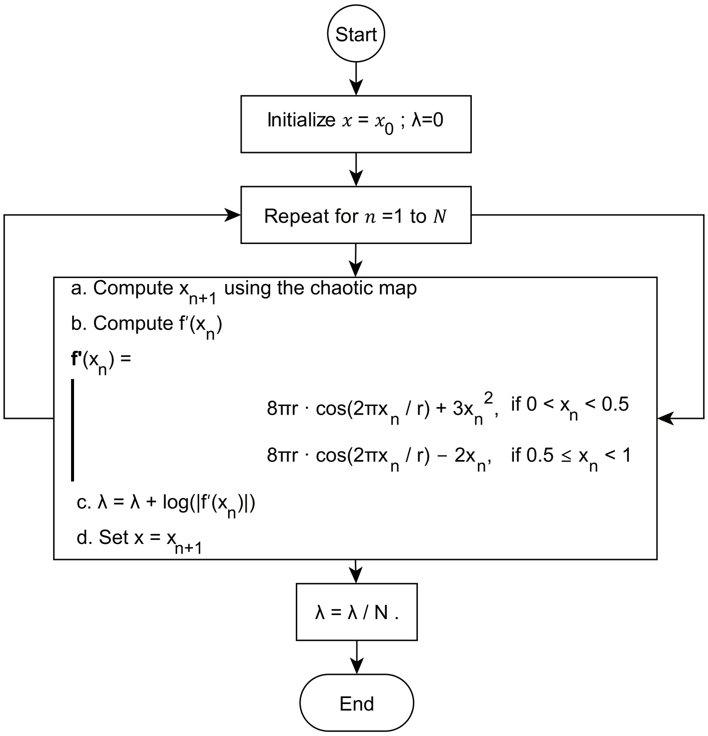
Start
Initialize $x = x_0$; λ=0
Repeat for n =1 to N
a. Compute x_{n+1} using the chaotic map
b. Compute $f'(x_n)$
$f'(x_n)$ =
$8\pi r \cdot \cos(2\pi x_n / r) + 3x_n^2$, if $0 < x_n < 0.5$
$8\pi r \cdot \cos(2\pi x_n / r) - 2x_n$, if $0.5 \le x_n < 1$
c. $\lambda = \lambda + \log(|f'(x_n)|)$
d. Set $x = x_{n+1}$
λ = λ / N .
End

Figure 3: Lyapunov Flowchart

Fig. 4 shows $\lambda > 0$ for $r > 0.55$, confirming chaos. Table 1 compares key properties; the proposed map yields $\lambda_{\max} = 5.04$ and broader key space ($r \in (0, 12)$), outperforming classical maps.

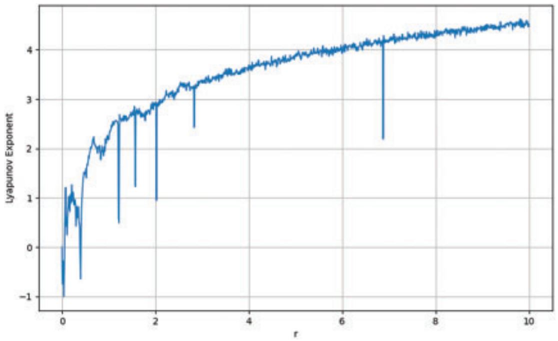

Figure 4: Lyapunov Exponent (λ) vs. Control Parameter (r) for the proposed SPCM

Table 1: Comparison of chaotic maps

Chaotic Map	$\lambda_{\max}$	Key Space
Proposed	5.04	$x_0 \in (0,1), r \in (0,12)$
[27]	4.50	$x_0 \in (0,1), r \in (0,9)$
[20]	4.88	$x_0 \in (0,1), \mu > 0, \beta > 0$
Logistic map	0.6931	$x_0 \in (0,1), r \in (3.57,4)$
Tent map	0.683	$x_0 \in (0,1), r \in (1,2)$
Sine map	0.560	$x_0 \in (0,1), r \in (0.87,1)$

The cobweb diagram [39] in Fig. 5a illustrates trajectory divergence from initial values at $x_0 = 0.2827727272727267$, $r = 11.884388888888877$, demonstrating high sensitivity and non-repeating nature characteristic of chaos. The 0-1 test [40] assesses randomness using: $p(n+1) = p(n) + \phi(n)\cos(cn)$ and $q(n+1) = q(n) + \phi(n)\sin(cn)$; with $K = \lim_{n\to\infty} \frac{\log M(n)}{\log n}$. $K \approx 1$ implies chaos. For the SPCM, $K = 0.9618$, and Fig. 5b shows Brownian-like motion, confirming complex dynamics. Entropy, $H(X) = -\sum_{i=1}^{n} p(x_i)\log p(x_i)$, quantifies unpredictability. The system achieves 3.8826 average entropy over 1000 iterations. Fig. 5c shows entropy variations over control parameter r, affirming strong randomness. The bifurcation diagram [41] (Fig. 5d) shows chaotic onset at $r > 0.55$. The resulting aperiodic trajectories and dense orbits confirm dynamic instability and complex nonlinear behavior.

Sensitivity examines how minor changes in initial conditions or parameters impact the system's output over time analysis [42]. Fig. 6a,b illustrates the system's sensitivity to the initial condition $x_0 = 0.2827727272727267$, perturbed by a tiny offset of $\delta_x = 10^{-15}$. Although the perturbation is negligible, the two resulting trajectories diverge rapidly after only a few iterations. This indicates that the system exhibits exponential divergence from nearly identical starting points, a hallmark of chaotic dynamics. Similarly, Fig. 6c,d depicts the effect of a small variation in the control parameter $r = 11.884388888888877$. Even a perturbation in the fifth or sixth decimal place causes drastically different long-term behavior. These results confirm the strong sensitivity of the SPCM to initial conditions and system parameters. In the context of cryptography, this property ensures that even minimal key or input changes produce entirely different encrypted outputs, thereby enhancing resistance to differential, brute-force, and reverse-engineering attacks.

The histograms shown in Fig. 7 illustrate the distinct behaviors of three chaotic maps, all initialized with $x_0 = 0.5$ and iterated 10,000 times for fair comparison. The Logistic Map ($r = 3.99$) exhibits classic chaotic behavior with a characteristic U-shaped distribution. The Sine Map ($\mu = 0.99$) reflects smoother, sinusoidal dynamics, concentrating values near the center. The proposed SPCM Map ($r = 11.8843$) reveals a more complex, nearly uniform distribution due to its piecewise, discontinuous design, capturing stronger chaotic behavior and enhanced trajectory mixing. This reflects the system's balance between randomness and structural control.

The proposed SPCM exhibits key chaotic properties such as ergodicity and mixing. Ergodicity ensures uniform coverage of the phase space, evident in the histograms (Fig. 7) and high entropy (Fig. 5c). Mixing implies statistical independence across iterations, supported by the discontinuity at $x_n = 0.5$ (Eq. (3)), high Lyapunov exponent (5.04), and 0-1 test score ($K \approx 0.9618$). These findings confirm SPCM's robustness for generating secure, pseudo-random sequences.

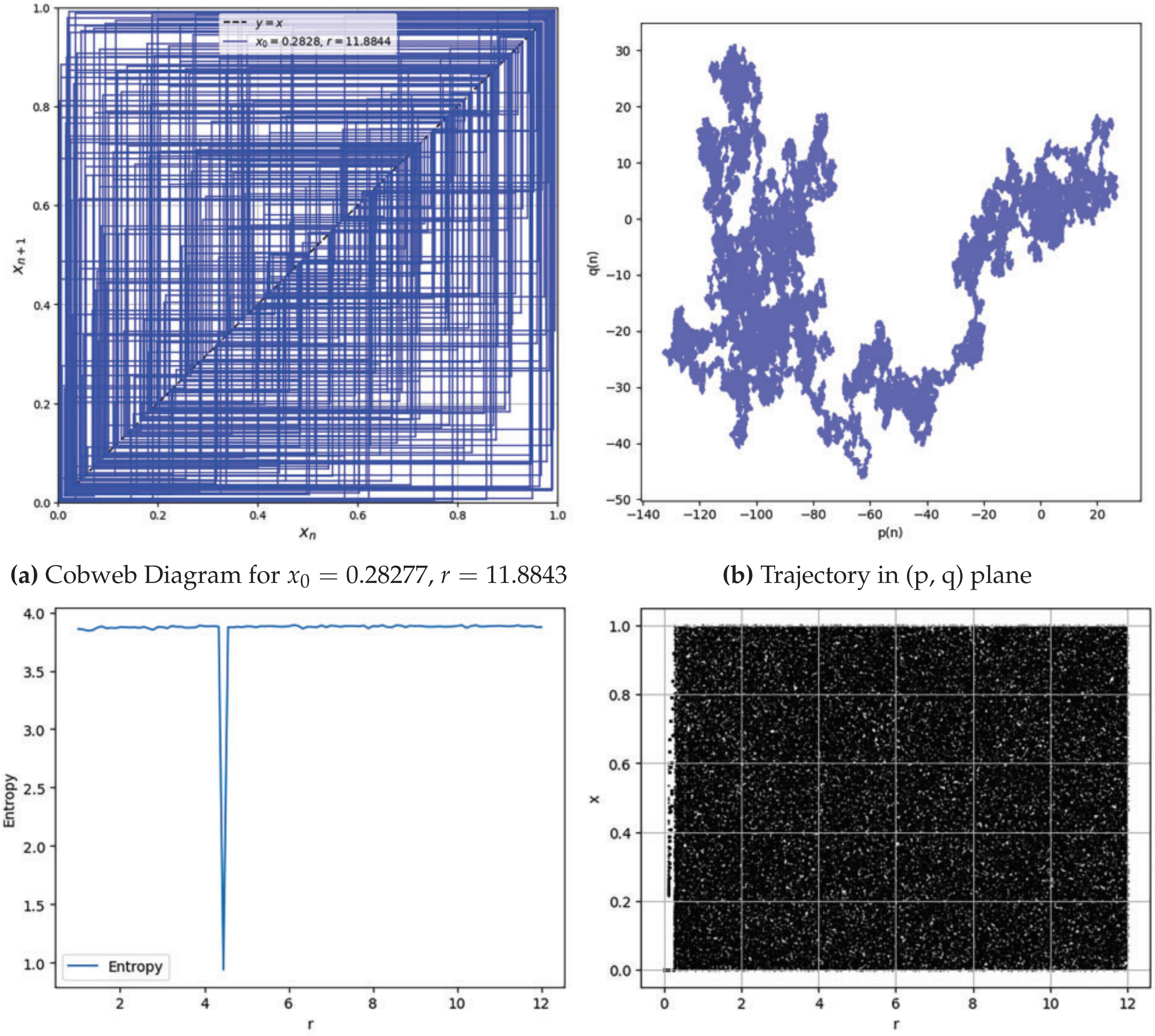

(a) Cobweb Diagram for $x_0 = 0.28277$, $r = 11.8843$

(b) Trajectory in (p, q) plane

(c) Entropy analysis of the proposed SPCM

(d) Bifurcation diagram for the proposed SPCM

Figure 5: Dynamic analysis of the proposed Sine-Polynomial Chaotic Map (SPCM). (a) Cobweb diagram showing the trajectory behavior of SPCM for x_0 = 0.28277 and r = 11.8843, confirming high sensitivity and chaoticity. (b) 0–1 test trajectory in the (p, q) plane, with Brownian-like motion and $K \approx 0.9618$, validating chaotic dynamics. (c) Entropy curve with respect to the control parameter r, demonstrating strong randomness and unpredictability. (d) Bifurcation diagram indicating chaotic behavior beyond $r > 0.55$, with dense, aperiodic orbits

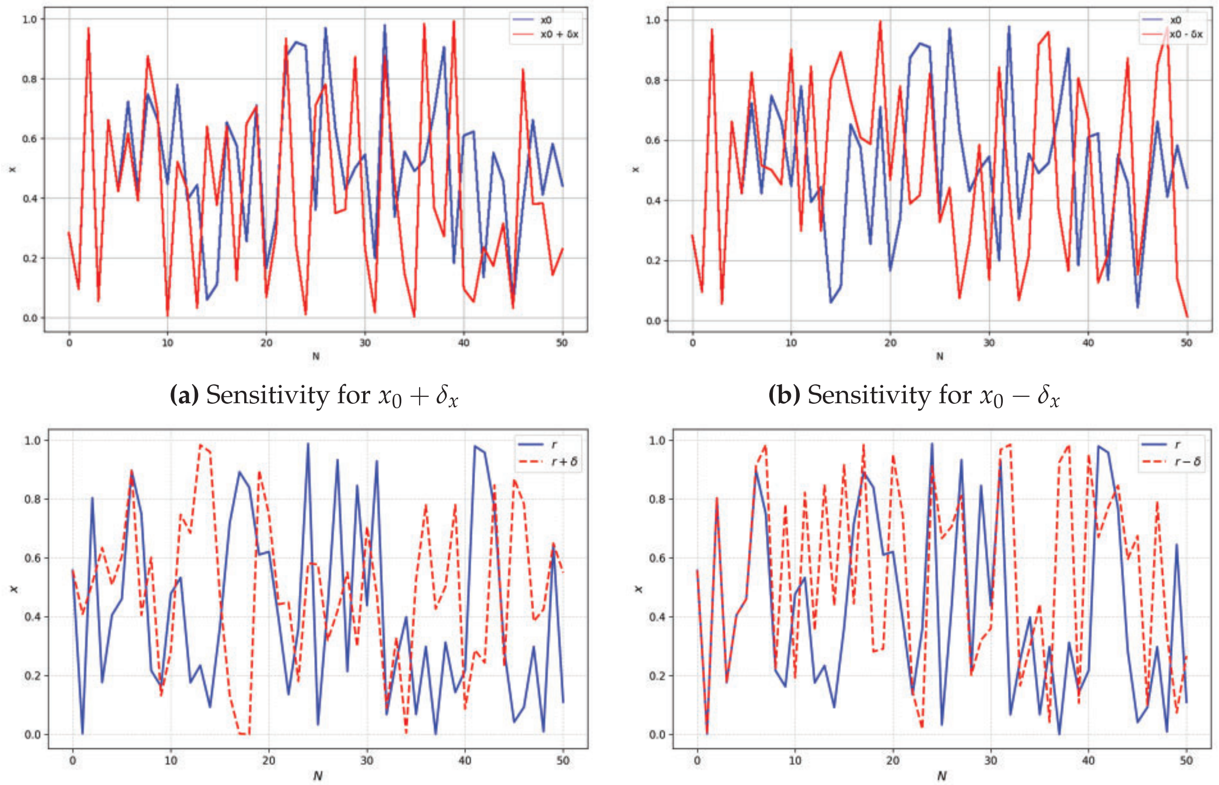

(a) Sensitivity for $x_0 + \delta_x$

(b) Sensitivity for $x_0 - \delta_x$

(c) Parameter Sensitivity $r + \delta_x$

(d) Parameter Sensitivity $r - \delta_x$

Figure 6: Sensitivity analysis of the proposed Sine-Polynomial Chaotic Map (SPCM). (a) Divergence of trajectories for initial condition perturbed by $\delta x = +10^{-15}$, showing significant deviation after a few iterations. (b) Divergence for $\delta x = -10^{-15}$, again confirming the system's extreme sensitivity to initial condition x_0. (c) Trajectory deviation due to a slight increase in control parameter r by $\delta r = +10^{-15}$, validating parameter sensitivity. (d) Divergence for $r - \delta r$, highlighting the robustness of the system's chaotic response to minimal parameter changes. The perturbation δx and δr represent minimal offsets ($\approx 10^{-15}$)

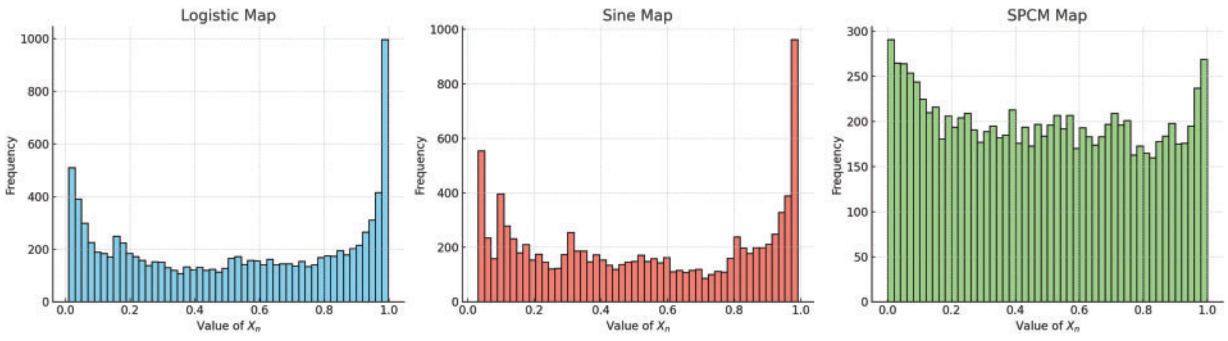

Figure 7: Histogram: Proposed SPCM, Sine and Logistic Maps

4.2 Performance Analysis Using NIST SP800-22R1A Test-Suit

The NIST SP800-22R1A Test Suite [43] is a comprehensive set of statistical tests used to evaluate the randomness of binary sequences, assessing components like frequency distribution, runs, entropy, and serial correlation. These tests help identify biases or trends that could compromise security, ensuring that binary sequences are suitable for cryptographic applications and simulations.

Table 2 summarizes the NIST SP800-22R1A test results for a binary sequence, covering all qualifying tests. All tests passed, confirming the sequence's high randomness and applicability for cryptographic applications.

Table 2: NIST SP800-22R1A Test Results for Sine-Polynomial Chaotic System

Test	*p*-val	Result	Test	*p*-val	Result
Monobit	0.561	✓	Serial	0.528	✓
Frequency Within Block	0.331	✓	Approximate Entropy	0.293	✓
Runs	0.944	✓	Cumulative Sums	0.714	✓
Longest Run of Ones	0.341	✓	Random Excursion	0.438	✓
DFT	0.412	✓	Random Excursion Variant	2.27	✓
Non-Overlapping Template	0.998	✓			

Note: Legend: ✓ Test Pass × Test Failed.

4.3 Performance Analysis Using Diehard Test-Suit

The performance of the proposed SPCM was rigorously evaluated using the Diehard tests suite, a collection of rigorous tests to assess the randomness of sequences. The SP Chaotic Map, with parameters $r = 11.878888888888889$ and $x_0 = 0.2772727272727273$, was used to generate a data set of 30,000,000 values. The results of the Diehard tests are summarized in Table 3. The Sine-Polynomial Chaotic System successfully passed all Diehard and NIST tests, demonstrating strong randomness and robust chaotic behavior. Its evaluation across multiple analyses confirms its suitability for cryptographic applications and secure communication systems.

Table 3: Diehard Test Results for Sine-Polynomial Chaotic System

Test Name	nt	ts	ps	*p*-val	Result	Test Name	nt	ts	ps	*p*-val	Result
diehard_birthdays	0	100	100	0.3599	✓	diehard_craps	0	200 K	100	0.4705	✓
diehard_operm5	0	1 M	100	0.7486	✓	marsaglia_tsang_gcd	0	10 M	100	0.1426	✓
diehard_rank_32x32	0	40 K	100	0.8824	✓	sts_monobit	1	100 K	100	0.3189	✓
diehard_bitstream	0	2 M	100	0.7097	✓	sts_runs	2	100 K	100	0.7528	✓
diehard_opso	0	2 M	100	0.9344	✓	rgb_bitdist	1	100 K	100	0.3759	✓
diehard_oqso	0	2 M	100	0.5740	✓	rgb_minimum_distance	2	10 K	1 K	0.8910	✓
diehard_dna	0	2 M	100	0.1785	✓	rgb_permutations	2	1 M	100	0.2786	✓
diehard_count_1s_str	0	256 K	100	0.3606	✓	rgb_lagged_sum	0	1 M	100	0.6031	✓
diehard_count_1s_byt	0	256 K	100	0.8298	✓	rgb_kstest_test	0	1 M	100	0.0074	⋆
diehard_parking_lot	0	12 K	100	0.1050	✓	dab_bytedistrib	0	512 K	100	0.4983	✓
diehard_3dsphere	3	4 K	100	0.8377	✓	dab_dct	256	500 K	100	0.8188	✓
diehard_squeeze	0	100 K	100	0.9464	✓	dab_filltree	32	500 K	100	0.9789	✓
diehard_sums	0	100	100	0.0292	✓	dab_filltree2	0	500 K	100	0.5054	✓
diehard_runs	0	100 K	100	0.0305	✓	dab_monobit2	12	65 M	100	0.9386	✓

Note: Legend: ✓ Test Pass ⋆ Test Weak × Test Failed.

4.4 Comparative Analysis of Test Coverage in Chaotic System Research

This subsection compares the test coverage of the proposed Chaotic System with existing studies. Table 4 summarizes key tests (rows) and their application across different studies (columns). The proposed system demonstrates more comprehensive and extensive evaluation, outperforming prior chaotic maps by covering a wider range of rigorous tests, thereby validating its robustness and suitability for cryptographic applications.

Table 4: Comparison of tests conducted for different chaotic maps

Test	Proposed	[14]	[15]	[20]	[44]	[24]	[27]	[28]
NIST SP800-22R1A tests	✓	×	×	✓	×	×	×	×
Bifurcation	✓	✓	✓	✓	×	✓	✓	✓
Lyapunov	✓	✓	✓	✓	✓	✓	✓	✓
Sensitivity test	✓	×	×	✓	×	×	×	×
Cobweb	✓	✓	×	✓	×	×	×	×
0-1 test	✓	×	×	✓	×	×	×	×
Histogram analysis	✓	×	×	✓	×	✓	×	×
Distribution of orbit lengths	×	✓	×	×	×	×	✓	×
Attractor phase diagram	×	×	×	×	✓	×	×	×
Iteration function diagrams	×	×	×	×	×	×	×	✓
Shannon's entropy	✓	×	×	×	×	×	×	✓
DieHard tests	✓	×	×	×	×	×	×	×

Note: Legend: ✓ Test Conducted × Test Not Conducted.

5 Application of Proposed SPCM

5.1 Encryption Key Generation

To generate the encryption key matrix, the SPCM (Eq. (3)) is employed using an initial value $x_0 \in (0, 1)$ and a control parameter $r \in (0, 12)$. The goal is to construct a 2D matrix of size 256 × 256, containing 8192 unique 8-bit values, corresponding to a 65,536-bit key (i.e., 8192 bytes) suitable for secure image encryption.

The chaotic system is first iterated to produce a sequence $\{x_k\}_{k=1}^{T}$ using Eq. (6), where each value is transformed into an 8-bit key using the mapping

$$K_{\text{flat}}(k) = \left\lfloor (x_k \cdot 10^{16}) \mod 256 \right\rfloor, \quad \text{for } k = 1, 2, \ldots, T \geq 8192. \tag{6}$$

Here, each chaotic value is scaled by a large factor to preserve precision, modulo operation is applied to restrict values to the range $[0, 255]$, and the floor function ensures integer truncation. Furthermore, uniqueness is enforced by extracting non-repeating elements from the sequence, resulting in $K_{\text{unique}} = \text{Unique}(K_{\text{flat}})$. It is ensured that the number of unique values satisfies the condition $|K_{\text{unique}}| \geq 8192$. If the condition is not met, the chaotic map continues to iterate until the required number of unique values is generated. Once the unique values are obtained, the 1D array is reshaped into a 2D matrix using the transformation defined in Eq. (7):

$$K(i, j) = K_{\text{unique}}[i \cdot 256 + j] \mod 256, \quad \text{for } i, j \in \{0, \ldots, 255\}. \tag{7}$$

This transformation maps the 1D sequence into a 2D structure while preserving the ordering. The resulting key matrix $K(i, j)$ consists of 8-bit values in the range $[0, 255]$, is fully unique, and can be directly used for pixel-level encryption, permutation, or other position-sensitive cryptographic operations (see visual representation in Fig. 8). The proposed SPCM-based encryption implements diffusion through chaotic pixel permutation and confusion through pixel-wise XOR with a chaotic key matrix, making the system resistant to statistical and differential attacks while maintaining computational efficiency for WSNs.

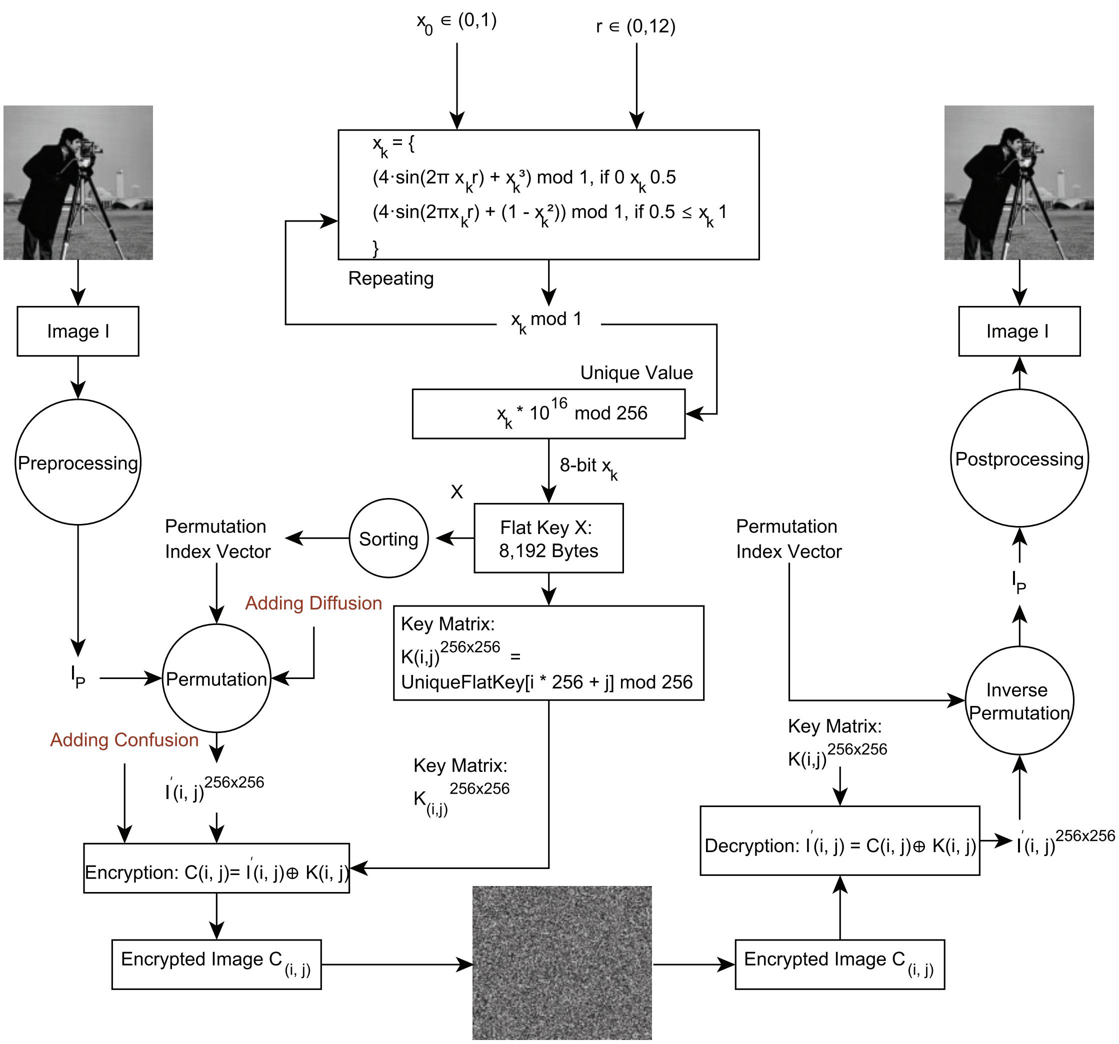
$x_0 \in (0,1)$
$r \in (0,12)$
x_k = {
$(4 \cdot \sin(2\pi\, x_k r) + x_k^3)$ mod 1, if 0 x_k 0.5
$(4 \cdot \sin(2\pi x_k r) + (1 - x_k^2))$ mod 1, if 0.5 ≤ x_k 1
}
Repeating
x_k mod 1
Unique Value
$x_k * 10^{16}$ mod 256
8-bit x_k
X
Flat Key X: 8,192 Bytes
Sorting
Permutation Index Vector
Adding Diffusion
Key Matrix: $K(i,j)^{256x256}$ = UniqueFlatKey[i * 256 + j] mod 256
Image I
Preprocessing
I_P
Permutation
Adding Confusion
$I'(i, j)^{256x256}$
Key Matrix: $K_{(i,j)}^{256x256}$
Encryption: C(i, j)= I'(i, j)⊕ K(i, j)
Encrypted Image $C_{(i, j)}$
Encrypted Image $C_{(i, j)}$
Decryption: I'(i, j) = C(i, j)⊕ K(i, j)
$I'(i, j)^{256x256}$
Key Matrix: $K(i,j)^{256x256}$
Permutation Index Vector
Inverse Permutation
I_P
Postprocessing
Image I

Figure 8: Key generation, image encryption and decryption process

5.2 Image Encryption

We employ chaos-based lightweight image encryption using an SPCM to secure images in WSNs. This approach leverages the sensitivity to initial conditions and nonlinear dynamics of chaotic systems to ensure strong security with minimal computational overhead, making it well-suited for resource-constrained environments. We begin by preprocessing the input image such that $I_p = \text{Preprocess}(I)$ where I denotes the original image and I_p represents the preprocessed version, typically resized and converted to grayscale. This step standardizes the input format and enhances the overall robustness of the encryption process. Next, we apply a chaotic permutation using a sequence X generated from the SPCM. By sorting X, we obtain a permutation index vector $\pi = \text{sort\_indices}(X)$ which we then use to reorder the pixels in I_p to get I' using permutation as $I' = P(I_p, \pi)$. This permutation step disrupts the spatial correlations within the image, thereby enhancing diffusion. During decryption, we apply the inverse permutation vector π^{-1} to accurately reconstruct the original pixel arrangement. Following permutation, we perform encryption using a key matrix $K(i,j)$, generated as described in Eq. (7), by applying a pixel-wise XOR operation (see Eq. (8)):

$$C(i,j) = I'(i,j) \oplus K(i,j) \tag{8}$$

Here, $K(i,j) \in \{0,1,\ldots,255\}$ is the chaotic key, $\oplus$ denotes the XOR operation, and $C(i,j)$ is the resulting encrypted pixel. This XOR operation introduces confusion, resulting in the final encrypted image C. To decrypt, we reverse the process: we apply the same chaotic key $K(i,j)$ via XOR to retrieve the permuted image I', and then use π^{-1} to recover I_p. This ensures that our encryption scheme is not only secure and efficient but also fully reversible (see Fig. 8).

5.3 *Encryption Analysis*

This section evaluates the proposed encryption technique using avalanche effect, entropy, and correlation coefficient analyses, encryption time, which are the key metrics for assessing encryption strength. The avalanche effect ensures small changes in input or key produce major ciphertext changes, improving resistance to Differential Attacks (DA). We tested perturbations of 10^{-14} on chaotic parameters x_0 and r using high-precision arithmetic with the "cameraman.png" image (256 × 256) (Fig. 8). Table 5 shows average bit difference ratios of 50.0094% for x_0 and 50.0388% for r, confirming strong avalanche behavior and validating robustness suitable for resource-constrained WSNs.

Table 5: Avalanche effect for perturbations in x_0 and r

Trial	x_0 Perturbation			r Perturbation		
	Original x_0	Perturbed x_0	Bit Diff. %	Original r	Perturbed r	Bit Diff. %
1	0.282772727272727	0.282772727272741	49.9392	11.8843888888888877	11.884388888888891	50.0805
2	0.282772727272727	0.282772727272719	50.1404	11.8843888888888877	11.8843888888888863	50.0032
3	0.282772727272727	0.282772727272735	49.9416	11.8843888888888877	11.8843888888888885	49.9554
4	0.282772727272727	0.282772727272712	49.9390	11.8843888888888877	11.8843888888888870	50.0605
5	0.282772727272727	0.282772727272738	49.9920	11.8843888888888877	11.8843888888888892	50.0605
6	0.282772727272727	0.282772727272720	50.0988	11.8843888888888877	11.8843888888888864	49.9554
7	0.282772727272727	0.282772727272732	49.9800	11.8843888888888877	11.8843888888888889	50.0490
8	0.282772727272727	0.282772727272715	50.0969	11.8843888888888877	11.884388888888871	50.0715
9	0.282772727272727	0.282772727272743	49.9962	11.8843888888888877	11.8843888888888893	50.0715
10	0.282772727272727	0.282772727272725	49.9702	11.8843888888888877	11.8843888888888862	50.0805

Histogram analysis checks pixel intensity distribution. A uniform histogram in the encrypted image (Fig. 9a) confirms effective pixel value randomization. The decrypted image histogram (Fig. 9b) shows clear peaks and valleys, reflecting correct image recovery. Entropy $H = -\sum_{i=0}^{255} p(i) \log_2 p(i)$ quantifies pixel randomness. For an 8-bit image, ideal entropy is 8 bits. The encrypted image entropy is 7.9961 bits, close to ideal, showing high randomness. The decrypted image entropy is 7.0097 bits, lower due to restored structure, confirming correct decryption.

Correlation coefficients between adjacent pixels (horizontal, vertical, diagonal) should approach zero in encrypted images, indicating minimal pixel relationship. They are computed as Correlation = $\frac{\mathrm{cov}(x,y)}{\sigma_x \sigma_y}$; where $\mathrm{cov}(x,y)$ is covariance and σ_x, σ_y are standard deviations.

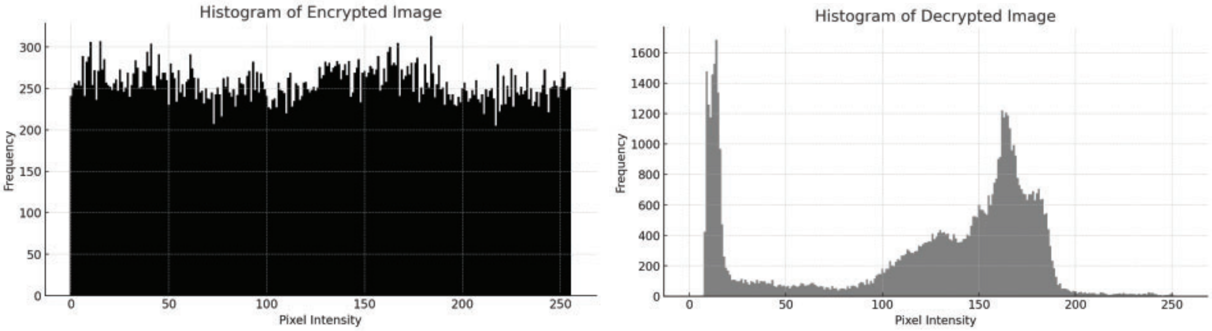

(a) Histogram of the Encrypted Image

(b) Histogram of the Decrypted Image

Figure 9: Histogram analysis of encrypted and decrypted images using the proposed SPCM-based encryption scheme. (a) Histogram of the encrypted image shows a uniform distribution of pixel intensities across the full grayscale range [0, 255], indicating strong randomness and high resistance to statistical attacks. (b) Histogram of the decrypted image restores the original non-uniform distribution with visible peaks and valleys, confirming successful image recovery and decryption accuracy

Encrypted image correlations: horizontal = 0.0033, vertical = 0.0002, diagonal = 0.0064, confirming effective decorrelation. Decrypted image correlations are high: horizontal = 0.9335, vertical = 0.9592, diagonal = 0.9087, indicating successful restoration of natural image structure, shown in Table 6.

Table 6: Correlation coefficients of adjacent pixels in original and encrypted images

Image	State	Horizontal	Vertical	Diagonal
Lena [45] (512 × 512)	Original	0.9721	0.9853	0.9602
	Encrypted	0.0031	0.0005	0.0058
Cameraman [45] (256 × 256)	Original	0.9345	0.9478	0.9123
	Encrypted	0.0033	0.0002	0.0064
Peppers [45] (512 × 512)	Original	0.9632	0.9789	0.9514
	Encrypted	0.0028	−0.0007	0.0051

The proposed algorithm demonstrates efficient encryption with an average time of 0.152582 s and throughput of 433.42 KB/s, showing consistent performance across trials. Encryption time varies between 0.135181 and 0.262618 s, indicating stable operation under different conditions. Table 7 compares this performance with existing algorithms reported in the literature. The proposed method outperforms others, achieving significantly lower encryption times than [25] (2.750966 s), [46] (4.98 s), [47] (1.1168 s), and even [17] (0.25 s). Its throughput and speed make it suitable for real-time applications, balancing performance and efficiency effectively.

Table 7: Comparison of encryption time with existing algorithms

Algorithm	Encryption Time [s]	Machine Specifications
Proposed	0.152582 (Avg.)	2.6 GHz Intel® Core™ i5, 8 GB RAM
[25]	2.750966	2.6 GHz Intel® Core™ i5, 8 GB RAM
[17]	0.25	2.6 GHz Intel® Core™ i5, 8 GB RAM

(Continued)

Table 7 (continued)

Algorithm	Encryption Time [s]	Machine Specifications
[47]	1.1168	2.6 GHz Intel® Core™ i5, 8 GB RAM
[48]	3.45	2.6 GHz Intel® Core™ i5, 8 GB RAM
[46]	4.98	2.6 GHz Intel® Core™ i5, 8 GB RAM
[16]	1.112	2.6 GHz Intel® Core™ i5, 8 GB RAM

5.4 Resistance to Cryptographic Attacks

To address the security requirements of resource-constrained WSNs, the proposed SPCM is evaluated for its resilience against Chosen-Plaintext Attacks (CPA), DA, and SA. The lightweight design of the one-dimensional SPCM ensures low computational complexity, making it suitable for WSNs while maintaining robust cryptographic properties.

5.4.1 CPA Resistance

The proposed SPCM-based encryption scheme demonstrates strong resistance to CPAs due to its inherent nonlinearity and dynamic key generation. The piecewise sine-polynomial transformation introduces nonlinear chaotic mixing, ensuring that even minor changes in plaintext lead to significantly different ciphertexts, as illustrated in Fig. 8. This diffusion effect effectively prevents an adversary from inferring any meaningful relationship between plaintext and ciphertext. Furthermore, the key matrix used for encryption is dynamically generated, consisting of 65,536 bits as detailed in Section 5.1. This matrix depends sensitively on the initial parameters x_0 and r, and any small variation in these parameters results in a completely different key stream. This sensitivity, combined with the high dimensionality of the key space, makes key recovery through known plaintext-ciphertext pair analysis computationally infeasible [49].

5.4.2 DA Resistance

The SPCM also exhibits robust resistance to DA. This is primarily evidenced by the strong avalanche effect observed during the encryption process. Specifically, perturbations in the initial parameters x_0 and r result in average bit difference ratios of 50.0094% and 50.0388%, respectively, as reported in Table 5. These values exceed the ideal threshold of 50%, confirming a highly effective diffusion mechanism [50]. Moreover, the nearly equal avalanche performance across both parameters indicates a uniformly distributed sensitivity throughout the chaotic system. This uniformity, also visualized in Fig. 8, ensures that the encryption scheme does not favor any specific direction of perturbation, making it resilient to differential cryptanalysis.

5.4.3 SA Resistance

To assess statistical resistance, the SPCM-based encryption was subjected to standard randomness tests. The encrypted outputs successfully passed all tests under the NIST SP800-22 suite, with p-values exceeding 0.01 as shown in Table 2, thereby validating the statistical randomness of the ciphertext. In addition, Diehard tests were conducted on binary sequences generated from SPCM orbits, achieving a 100% pass rate (Table 3). Beyond these formal tests, the scheme also demonstrates practical resistance to SA through its decorrelation capability. The correlation coefficients of adjacent pixels in the encrypted images were consistently observed to be below 0.0064 (Section 5.3), effectively eliminating detectable patterns and resisting frequency-based analysis. These results collectively affirm that the proposed scheme provides a high level of security against statistical cryptanalysis.

5.5 *Resource Efficiency Analysis*

This subsection presents an analytical evaluation of the proposed encryption algorithm's computational, energy, and memory efficiency using the TelosB wireless sensor platform (MSP430F1611 @ 8 MHz) as a reference. The estimates are derived from instruction-level energy metrics published in the MSP430F1611 datasheet and validated benchmark studies [51,52] (Table 8). Although the algorithm has not yet been deployed on physical motes, this modeling approach aligns with standard practices in lightweight cryptographic analysis and pre-deployment feasibility assessments for WSNs. Future work will include experimental validation using Contiki-NG or TinyOS-based TelosB platforms.

Table 8: Unit costs (MSP430F1611)

Parameter	Value
Active mode energy per cycle	0.013 μJ
Flash write energy per byte	0.0349 mJ
Flash read energy per byte	0.015 mJ

The computational complexity of the proposed security framework arises primarily from three stages: key generation, permutation vector computation, and XOR-based encryption. Key generation using the SPCM is linear, $O(n)$, though may increase to $O(n \log n)$ when uniqueness filtering is applied. Permutation vector generation involves sorting, also incurring $O(n \log n)$, while pixel-wise XOR encryption operates in $O(n)$. Hence, the overall complexity is $O(n \log n)$.

The energy cost of the proposed SPCM-based image encryption scheme for a 256 × 256 image (8192 bytes) comprises three main components: key generation, permutation index sorting, and pixel-wise XOR encryption. Key generation employs the sine-polynomial chaotic map, where each iteration involves approximately 8 operations that are 1 multiplication, 1 sine function, 2–3 arithmetic operations (addition, subtraction, power), and 1 modulus. These are summed to about 8 arithmetic units per iteration, which are assumed to take 8 clock cycles. To produce 8192 unique 8-bit values, 8192 iterations are performed, resulting in $8192 \times 8 = 65{,}536$ cycles. At an active mode energy of 0.013 μJ per cycle, this stage consumes approximately $65{,}536 \times 0.013\,\mu\text{J} = 0.852\,\text{mJ}$. For pixel permutation, the chaotic sequence is sorted to generate the index vector, requiring $O(n \log n)$ operations, with $n = 8192$. This results in $8192 \times \log_2 8192 = 8192 \times 13 = 106{,}496$ cycles, consuming $106{,}496 \times 0.013\,\mu\text{J} = 1.384\,\text{mJ}$. Finally, encryption applies an XOR between each image pixel and its corresponding key byte. This involves 8192 XOR operations, each assumed to take one cycle, costing $8192 \times 0.013\,\mu\text{J} = 0.1065\,\text{mJ}$. Summing these, the total energy required for a complete encryption operation is approximately $0.852 + 1.384 + 0.1065 =$ **2.34 mJ**, demonstrating the scheme's suitability for energy-constrained platforms such as WSNs.

Memory usage comprises 8 KB for the key matrix and 1.2 KB for buffers, totaling less than 10 KB well below the TelosB's 48 KB RAM capacity. Compared to the estimated 2.8 mJ energy cost of AES-128 on TelosB-class hardware [34,35], the proposed scheme consumes approximately 2.34 mJ, representing a 16.4% reduction in energy consumption while maintaining comparable security through chaotic diffusion properties.

In terms of memory, AES-128 implementations on MSP430-class motes typically require around 10–12 KB, largely due to S-box lookup tables and key expansion operations [33]. ECC-based encryption, while offering asymmetric key advantages, typically demands over 80,000 cycles for a single scalar multiplication and uses more than 12 KB RAM for modular arithmetic and key storage [35,53]. By contrast, our

SPCM scheme completes encryption in under 175,000 cycles and uses less than 10 KB memory, making it more appropriate for frequent operations in resource-constrained WSN nodes.

5.6 Comparison of Chaos-Based Image Encryption in WSNs

Table 9 compares the proposed SPCM with three existing chaos-based encryption methods for WSNs across seven criteria: 1) chaotic model type, 2) key space size, 3) encryption speed, 4) Lyapunov exponent (measuring chaos strength), 5) energy consumption, 6) throughput, and 7) resistance to cryptographic attacks. The SPCM demonstrates competitive advantages in chaos complexity (highest Lyapunov exponent), energy efficiency (lowest mJ/image), and throughput (fastest KB/s), while maintaining robust security against multiple attack types. Comparisons are drawn from cited peer-reviewed works to contextualize SPCM's performance within the field.

Table 9: Comparison of chaos-based image encryption techniques in WSNs

Criteria	SPCM (Proposed)	[54]	[55]	[56]
Chaos model	Sine-Polynomial	Logistic	Hybrid (Henon+SINE)	Arnold Cat Map
Key space	7.9×10^{35}	10^{14}	10^{28}	10^{20}
Encryption time (ms)	152.58	320.50	198.40	225.30
Lyapunov exponent	5.04	0.693	4.91	3.20
Energy (mJ)	2.34	Not reported	Not reported	Not reported
Throughput (KB/s)	433.42	185.20	387.15	352.60
Attack resistance	CPA/DA	CPA	DA	CPA

6 Limitations

The proposed SPCM for WSN image encryption faces scalability limitations when applied to large-scale data, such as video encryption, which requires further experimental validation. Additionally, encryption performance metrics (e.g., 0.152582 s encryption time, 433.42 KB/s throughput) are hardware-specific, necessitating cross-platform testing to ensure robustness and consistency across diverse WSN environments.

7 Conclusion

This study presents SPCM, a chaotic system for image encryption in resource-constrained WSNs. By integrating sine and polynomial dynamics with a discontinuity at $x_n = 0.5$, SPCM ensures wide chaos ($r \in [0, 12]$) and strong key diversity (7.9×10^{35} keys), achieving 39% reduction in encryption time (0.152 s vs. 0.25 s in [17]) and 134% higher throughput (433.42 KB/s vs. 185.20 KB/s in [25]) than state-of-the-art chaotic alternatives. Its ergodic and mixing behavior, validated by NIST/Diehard tests and a Lyapunov exponent of 5.04, provides uniform phase space coverage. It furthermore provides resistance to CPA, DA and SA attacks, which is crucial for WSN applications. SPCM's lightweight performance (2.34 mJ/image) further demonstrates its practicality for energy-limited nodes. Future work should explore higher-dimensional extensions for scalable multimedia encryption and strengthen theoretical foundations, while securely exchanging parameters (x_0, r) via Elliptic Curve Diffie-Hellman (ECDH) or out-of-band methods.

Acknowledgement: The authors would like to thank the School of Electrical Engineering and Computer Science at GIST and the Department of Computer Science and Engineering at Chungnam National University for their support and collaborative environment during this research.

Funding Statement: This work was supported by the National Research Foundation of Korea (NRF) grant funded by the Korean government Ministry of Science and ICT (MIST) (RS-2022-00165225).

Author Contributions: The authors confirm contribution to the paper as follows: conceptualization, software implementation, writing, reviewing, editing, final drafting: David S. Bhatti, Annas W. Malik; supervision: David S. Bhatti; reviewing, formal analysis: Haeung Choi; reviewing, funding acquisition: Ki-Il Kim. All authors reviewed the results and approved the final version of the manuscript.

Availability of Data and Materials: The datasets and code supporting the findings of this study are available from the corresponding authors upon reasonable request.

Ethics Approval: Not applicable. This study did not involve human participants or animal subjects.

Conflicts of Interest: The authors declare no conflicts of interest to report regarding the present study.

References

1. Kandris D, Nakas C, Vomvas D, Koulouras G. Applications of wireless sensor networks: an up-to-date survey. Appl Syst Innov. 2020;3(1):14. doi:10.3390/asi3010014.
2. Kaddi M, Omari M, Alnatoor M. EECLP: a wireless sensor networks energy efficient cross-layer protocol. Comput Mater Contin. 2024;80(2):2611–31. doi:10.32604/cmc.2024.052048.
3. Bhatti DS, Saleem S, Imran A, Kim HJ, Kim KI, Lee KC. Detection and isolation of wormhole nodes in wireless ad hoc networks based on post-wormhole actions. Sci Rep. 2024 Feb;14(1):3428. doi:10.1038/s41598-024-53938-9.
4. Singh AP, Luhach AK, Gao XZ, Kumar S, Roy DS. Evolution of wireless sensor network design from technology centric to user centric: an architectural perspective. Int J Distrib Sens Netw. 2020;16(8):155014772094913. doi:10.1177/1550147720949138.
5. Verhulst F. Henri poincaré's inventions in dynamical systems and topology. In: Skiadas C, editor. The foundations of chaos revisited: from poincaré to recent advancements. understanding complex systems. Cham, Switzerland: Springer; 2016. p. 1–25. doi:10.1007/978-3-319-29701-9_1.
6. Aubin D, Dalmedico AD. Writing the history of dynamical systems and chaos: longue durée and revolution, disciplines and cultures. Historia Mathematica. 2002;29(3):273–339. doi:10.1006/hmat.2002.2351.
7. Bishop R. Chaos. In: Zalta EN, Nodelman U, editors. The stanford encyclopedia of philosophy. Winter 2024 ed. Metaphysics Research Lab, Stanford University; 2024 [Internet]. [cited 2025 Jul 24]. Available from: https://plato.stanford.edu/archives/win2024/entries/chaos/.
8. Jørgensen SE. Chaos. In: Jørgensen SE, Fath BD, editors. Encyclopedia of ecology. Oxford, UK: Academic Press; 2008. p. 550–1.
9. Kari AP, Navin AH, Bidgoli AM, Mirnia M. A novel multi-image cryptosystem based on weighted plain images and using combined chaotic maps. Multimed Syst. 2021;27(5):907–25. doi:10.1007/s00530-021-00772-y.
10. Biswas HR, Hasan MM, Bala SK. Chaos theory and its applications in our real life. Barishal Univ J Part. 2018;1(5):123–40.
11. Lawnik M, Moysis L, Volos C. A family of 1D chaotic maps without equilibria. Symmetry. 2023;15(7):1311. doi:10.3390/sym15071311.
12. Zhou Y, Hua Z, Pun CM, Philip Chen CL. Cascade chaotic system with applications. IEEE Trans Cybern. 2015;45(9):2001–12. doi:10.1109/TCYB.2014.2363168.
13. Hua Z, Zhang Y, Zhou Y. Two-dimensional modular chaotification system for improving chaos complexity. IEEE Trans Signal Process. 2020;68:1937–49. doi:10.1109/TSP.2020.2979596.
14. Lambić D. A new discrete-space chaotic map based on the multiplication of integer numbers and its application in S-box design. Nonlinear Dyn. 2020;100(1):699–711. doi:10.1007/s11071-020-05503-y.
15. Shafique A. A new algorithm for the construction of substitution box by using chaotic map. Eur Phys J Plus. 2020;135(2):194. doi:10.1140/epjp/s13360-020-00187-0.

16. Zhang X, Wang L, Wang Y, Niu Y, Li Y. An image encryption algorithm based on hyperchaotic system and variable-step josephus problem. Int J Optics. 2020;2020(1):6102824–15. doi:10.1155/2020/6102824.
17. Ali TS, Ali R. A new chaos based color image encryption algorithm using permutation substitution and Boolean operation. Multimed Tools Appl. 2020;79(27):19853–73. doi:10.1007/s11042-020-08850-5.
18. Li H, Yu C, Wang X. A novel 1D chaotic system for image encryption, authentication and compression in cloud. Multimed Tools Appl. 2021;80(6):8721–58. doi:10.1007/s11042-020-10117-y.
19. Fadhil MS, Farhan AK, Fadhil MN. Designing substitution box based on the 1D logistic map chaotic system. In: IOP Conference Series: Materials Science and Engineering. Vol. 1076. Bristol, UK: IOP Publishing; 2021.
20. Cheng Z, Wang W, Dai Y, Li L. Novel one-dimensional chaotic system and its application in image encryption. Complexity. 2022;2022(1):31. doi:10.1155/2022/1720842.
21. Zhang Y, Zhao J, Zhang B. An image encrypting algorithm based on 1D and 2D logistic chaotic systems. Int J Embed Syst. 2022;15(1):34–43. doi:10.1504/IJES.2022.122057.
22. Mondal B, Singh JP. A lightweight image encryption scheme based on chaos and diffusion circuit. Multimed Tools Appl. 2022;81(24):34547–71. doi:10.1007/s11042-021-11657-7.
23. Liu L, Wang J. A cluster of 1D quadratic chaotic map and its applications in image encryption. Math Comput Simul. 2023;204(12):89–114. doi:10.1016/j.matcom.2022.07.030.
24. Chen C, Zhu D, Wang X, Zeng L. One-dimensional quadratic chaotic system and splicing model for image encryption. Electronics. 2023;12(6):1325. doi:10.3390/electronics12061325.
25. Alexan W, Elkandoz M, Mashaly M, Azab E, Aboshousha A. Color image encryption through chaos and kaa map. IEEE Access. 2023;11:11541–54. doi:10.1109/ACCESS.2023.3242311.
26. Ding Y, Liu W, Wang H, Sun K. A new class of discrete modular memristors and application in chaotic systems. Eur Phys J Plus. 2023;138(7):638. doi:10.1140/epjp/s13360-023-04242-4.
27. Malik AW, Zahid AH, Bhatti DS, Kim HJ, Kim KI. Designing S-box using tent-sine chaotic system while combining the traits of tent and sine map. IEEE Access. 2023;11:79265–74. doi:10.1109/ACCESS.2023.3298111.
28. Alawida M. Enhancing logistic chaotic map for improved cryptographic security in random number generation. J Inf Secur Appl. 2024;80(1):103685. doi:10.1016/j.jisa.2023.103685.
29. Jain K, Titus B, Krishnan P, Sudevan S, Prabu P, Alluhaidan AS. A lightweight multi-chaos-based image encryption scheme for IoT Networks. IEEE Access. 2024;12(6):62118–48. doi:10.1109/ACCESS.2024.3377665.
30. Kıran HE. A novel chaos-based encryption technique with parallel processing using CUDA for mobile powerful GPU control center. Chaos Fract. 2024;1(1):6–18. doi:10.69882/adba.chf.2024072.
31. Archana G, Goyal R, Kumar KM. Blockchain-driven optimized chaotic encryption scheme for medical image transmission in IoT-Edge environment. Int J Comput Intell Syst. 2025;18(1):11. doi:10.1007/s44196-024-00731-1.
32. Hu LL, Chen MX, Wang MM, Zhou NR. Visually meaningful triple images encryption algorithm based on 2D compressive sensing and multi-region embedding. Knowl Based Syst. 2025;324(10):113804. doi:10.1016/j.knosys.2025.113804.
33. Hung CW, Hsu WT. Power consumption and calculation requirement analysis of AES for WSN IoT. Sensors. 2018;18(6):1675. doi:10.3390/s18061675.
34. Alkalbani AS, Mantoro T, Tap AOM. Comparison between RSA hardware and software implementation for WSNs security schemes. In: Proceeding of the 3rd International Conference on Information and Communication Technology for the Moslem World (ICT4M) 2010; 2010 Dec 13–14; Jakarta, Indonesia. p. E84–9.
35. Wang H, Li Q. Efficient implementation of public key cryptosystems on MICAz and TelosB motes. In: Technical report. USA: College of William and Mary; 2006. WM-CS-2006-07. doi:10.1007/11935308_37.
36. Liu Z, Jiang G, Wu Y, Wang T, Liu S, Ouyang Z. K-coverage estimation for irregular targets in wireless visual sensor networks deployed in complex region of interest. IEEE Sens J. 2025;25(10):18370–83. doi:10.1109/JSEN.2025.3558041.
37. Avrutin V, Gardini L, Sushko I, Tramontana F. Continuous and discontinuous piecewise-smooth one-dimensional maps. Singapore: World Scientific; 2019. doi:10.1142/8285.
38. Dingwell JB. Lyapunov exponents. Wiley encyclopedia of biomedical engineering. Hoboken, NJ, USA: John Wiley & Sons, Inc.; 2006. doi:10.1002/9780471740360.ebs0702.

39. Tomida AG. Matlab toolbox and GUI for analyzing one-dimensional chaotic maps. In: 2008 International Conference on Computational Sciences and its Applications; 2008 Jun 30–Jul 3; Perugia, Italy: IEEE. p. 321–30.
40. Gottwald GA, Melbourne I. The 0-1 test for chaos: a review. In: Chaos detection and predictability. Berlin/Heidelberg, Germany: Springer; 2016. p. 221–47. doi:10.1007/978-3-662-48410-4_7.
41. Jafari A, Hussain I, Nazarimehr F, Golpayegani SMRH, Jafari S. A simple guide for plotting a proper bifurcation diagram. Int J Bifurcat Chaos. 2021;31(1):2150011. doi:10.1142/S0218127421500115.
42. Lea DJ, Allen MR, Haine TW. Sensitivity analysis of the climate of a chaotic system. Tellus A Dyn Meteorol Oceanogr. 2000;52(5):523–32. doi:10.3402/tellusa.v52i5.12283.
43. Bassham LE, Rukhin AL, Soto J, Nechvatal JR, Smid ME, Barker EB, et al. SP 800-22 Rev. 1a: a statistical test suite for random and pseudorandom number generators for cryptographic applications. Gaithersburg, MD, USA: National Institute of Standards and Technology (NIST); 2010. NIST Special Publication 800-22 Revision 1a [Internet]. [cited 2025 Jul 24]. Available from: https://csrc.nist.gov/publications/detail/sp/800-22/rev-1a/final.
44. Wu R, Gao S, Wang X, Liu S, Li Q, Erkan U, et al. AEA-NCS: an audio encryption algorithm based on a nested chaotic system. Chaos Soliton Fract. 2022;165(3):112770. doi:10.1016/j.chaos.2022.112770.
45. MathWorks. MATLAB Image Processing Toolbox Standard Images (Lena, Cameraman, Peppers) [Internet]. [cited 2025 Jul 3]. Available from: https://www.mathworks.com/help/images/ref/.
46. Xu L, Li Z, Li J, Hua W. A novel bit-level image encryption algorithm based on chaotic maps. Optics Lasers Eng. 2016;78(2):17–25. doi:10.1016/j.optlaseng.2015.09.007.
47. Gong L, Qiu K, Deng C, Zhou N. An image compression and encryption algorithm based on chaotic system and compressive sensing. Opt Laser Technol. 2019;115(1):257–67. doi:10.1016/j.optlastec.2019.01.039.
48. Hu X, Wei L, Chen W, Chen Q, Guo Y. Color image encryption algorithm based on dynamic chaos and matrix convolution. IEEE Access. 2020;8:12452–66. doi:10.1109/ACCESS.2020.2965740.
49. Forrié R. The strict avalanche criterion: spectral properties of Boolean functions and an extended definition. In: Advances in Cryptology—CRYPTO'88: Proceedings 8. Cham, Switzerland: Springer; 1990. p. 450–68.
50. Webster AF, Tavares SE. On the design of S-boxes. In: Conference on the Theory and Application of Cryptographic Techniques. Cham, Switzerland: Springer; 1985. p. 523–34.
51. Instruments T. MSP430F161x Mixed Signal Microcontroller. Dallas, TX, USA; 2013 [Internet]. [cited 2025 Jul 24]. Available from: https://www.ti.com/lit/ds/symlink/msp430f1611.pdf.
52. Rafik MBO, Feham M. Performance evaluation on TelosB mote of a secure data aggregation protocol using ECC. In: Conference Nationale sur les Technologies de l'Information et les Telecommunications; 2013 Dec 10–11; Tlemcen, Algeria.
53. Gura N, Patel A, Wander A, Eberle H, Shantz SC. Comparing elliptic curve cryptography and RSA on 8-bit CPUs. In: Cryptographic hardware and embedded systems-CHES 2004. Berlin/Heidelberg, Germany: Springer; 2004. p. 119–32 doi:10.1007/978-3-540-28632-5_9.
54. Wang J, Han K, Fan S, Zhang Y, Tan H, Jeon G, et al. A logistic mapping-based encryption scheme for wireless body area networks. Future Gener Comput Syst. 2020;110(3):57–67. doi:10.1016/j.future.2020.04.002.
55. Yogi B, Khan AK, Roy S. Hybrid image encryption for IoT applications: integrating cellular automata and henon map to improve security and performance. In: 2024 4th International Conference on Technological Advancements in Computational Sciences (ICTACS); 2024 Nov 13–15; Tashkent, Uzbekistan. p. 1303–9.
56. Mondal B, Mandal T, Khan DA, Choudhury T. A secure image encryption scheme using chaos and wavelet transformations. Recent Pat Eng. 2018;12(1):5–14. doi:10.2174/1872212111666170223165916.